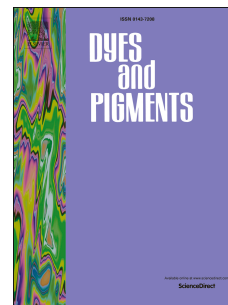


Accepted Manuscript

Proton transfer assisted facile encapsulation of picric acid in sol-gel derived silica decorated with azo-azomethine hosts

Ruchi Mutneja, Raghubir Singh, Varinder Kaur, Jörg Wagler, Edwin Kroke, Sushil Kumar Kansal



PII: S0143-7208(16)30701-X

DOI: [10.1016/j.dyepig.2016.12.060](https://doi.org/10.1016/j.dyepig.2016.12.060)

Reference: DYPI 5687

To appear in: *Dyes and Pigments*

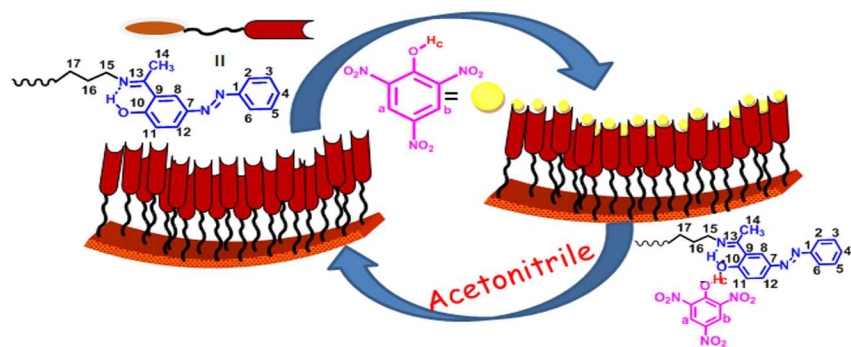
Received Date: 10 September 2016

Revised Date: 25 November 2016

Accepted Date: 21 December 2016

Please cite this article as: Mutneja R, Singh R, Kaur V, Wagler J, Kroke E, Kansal SK, Proton transfer assisted facile encapsulation of picric acid in sol-gel derived silica decorated with azo-azomethine hosts, *Dyes and Pigments* (2017), doi: 10.1016/j.dyepig.2016.12.060.

This is a PDF file of an unedited manuscript that has been accepted for publication. As a service to our customers we are providing this early version of the manuscript. The manuscript will undergo copyediting, typesetting, and review of the resulting proof before it is published in its final form. Please note that during the production process errors may be discovered which could affect the content, and all legal disclaimers that apply to the journal pertain.



1 Proton transfer assisted facile encapsulation of picric acid in sol-gel derived silica decorated
2 with azo-azomethine hosts

3 Ruchi Mutneja^a, Raghubir Singh^{b*}, Varinder Kaur^{a*}, Jörg Wagler^c, Edwin Kroke^c, Sushil
4 Kumar Kansal^d

5 ^aDepartment of Chemistry, Panjab University, Chandigarh – 160 014, India

6 ^bDAV College, Sector 10, Chandigarh – 160 010, India

7 ^cInstitut für Anorganische Chemie, Technische Universität Bergakademie, Freiberg – 09596
8 Freiberg, Germany

9 ^dDr. S. S. Bhatnagar University Institute of Chemical Engineering & Technology, Panjab
10 University, Chandigarh-160014, India

11 **Abstract:**

12 An azo-azomethine host has been synthesized and incorporated onto sol-gel derived
13 silica via hydrolysis of its tricyclic silanizing unit (i.e., a silatrane moiety). The azo-
14 azomethine functionalized silatrane (the “host”) was studied by various spectroscopic
15 techniques, elemental analysis, single crystal X-ray diffraction and thermogravimetric
16 analysis. Upon application to silica, significant change in surface area, pore diameter and
17 pore volume of the product confirmed the incorporation of azo-azomethine pendants in the
18 channels of the silica gel. Scanning electron microscopy and high resolution-transmission
19 electron microscopy were used to analyse the surface morphology and porous nature of the
20 sorbent. The azo-azomethine functionalized silica was further utilized for the uptake of picric
21 acid (PA) assisted by proton transfer. PA (the “guest”) being highly acidic interacts with the
22 electron rich site of the host via proton transfer. As a consequence electrostatic interactions
23 between host and guest molecules result in the fast uptake of PA onto the sorbent. Formation
24 of the host-guest complex was studied by NMR spectroscopy of the host/guest solutions and
25 host solutions with related dummy guest molecules. The maximum adsorption capacity of the
26 sorbent for PA was found to be 68.5 mg.g⁻¹ calculated on the basis of a Langmuir model.

27 **Key words:** Azo-azomethine, silatrane, proton transfer interaction, picric acid

28 **Corresponding author:**

29 raghu_chem2006@yahoo.com, var_ka04@yahoo.co.in

30 Contact no. 09872313583 (R. Singh), 09815065809 (V. Kaur)

31

32

1 1. Introduction

2 The pervasive utilization of picric acid (PA), e.g., as antiseptic in pharmaceutical
3 drugs, in electric batteries, leather industry, dye industries and as an explosive in fireworks
4 and weapons [1-6], caused (and still causes) its continuous release in the environment. Being
5 non-biodegradable, its sustained exposure to living beings may cause headache, nausea,
6 dizziness, difficulty in swallowing, diarrhoea, vomiting, shock, convulsions and disorders in
7 central nervous system, liver and kidneys [7-9]. Thus, development of new hosts for the
8 uptake of PA is most desirable for environment and health safety.

9 The electron deficient and highly acidic nature of PA (caused by its three electron
10 withdrawing nitro groups) is responsible for its active participation in charge transfer (CT)
11 and proton transfer (PT) reactions [10-13], thereby providing opportunities for development
12 of hosts for its detection/recognition. Based upon CT interactions, i.e., where electrons from
13 π electron rich molecular systems (as a “host”) are transferred to electron deficient PA (as a
14 “guest”) to form electron donor-acceptor (host-guest) interactions, various tweezers have
15 been developed in the past for the encapsulation and chemosensing of PA [14-19]. In hosts
16 involving CT accompanied by PT, formation of intermolecular hydrogen bond takes place
17 between hydroxyl group of PA (guest) with the electron rich site of a “host”, thereby
18 transferring its acidic proton. This generates picrate ions and a positively charged host site,
19 which augments the ionic host-guest interactions [20-22]. Previously, this type of molecular
20 hosts for PA have been developed utilizing proton accepting sites such as pyridine substituted
21 *p*-phenylenevinylene, dimethylamine group of *N,N*-dimethylaminocinnamaldehyde, and
22 1,3,5-tris(4'-(*N,N*-dimethylamino)phenyl)benzene [23-25]. It is envisaged herein that such
23 host-guest interactions may be probed for the adsorption of PA using a solid sorbent
24 functionalized with hosts having either proton accepting sites and/or π -electron rich sites.

25 Till date, some materials have been designed for the adsorption of PA such as
26 uncalcined MCM-14 [26] (with hydrophobic sites created by the surfactant template), and
27 cetyltrimethylammonium bromide (CTAB) coated magnetic iron oxide nanoparticles [27]
28 where ion pair formation between CTA^+ and picrate ions is responsible for adsorption under
29 acidic and basic conditions, respectively. Besides, electrostatic interactions are also
30 responsible in almond shell non-magnetic and magnetic activated carbon [28], and different
31 inorganic surfaces [29,30]. However, in Amberlite IRA-67 (a weakly basic gel-type
32 polyacrylic resin having tertiary amine functional group), acid-amine complex formation
33 through the transfer of acidic proton to the amine is accountable for the PA adsorption [31].

1 Amongst sorbents silica surfaces have been devoted major attention due to their
2 biocompatibility, large surface area as well as high thermal and chemical stability [32-35].
3 Because of its in general large adsorption capacity, tunable pore size, simple synthetic
4 accessibility and cost effectiveness [36,37], grafted mesoporous silica has been recognized as
5 efficient sorbent for the removal of heavy metal ions and toxic organic compounds [38-42].
6 Especially monolithic silica varieties with hierarchical porosity have gained much attention
7 due to their fascinating structure and wide application in chromatographic columns,
8 adsorption, enzyme immobilization, and catalytic supports [43-46]. Recently, Huesing et.al
9 reviewed and reported different strategies to synthesize monolithic materials with diverse
10 dimensions [47-50]. In porous silica surfaces, tethering of specific organic components is
11 generally achieved either by direct co-condensation method or post synthesis method
12 (grafting) [51-53]. In addition to condensation approaches, thiol-ene chemistry between an
13 olefin and a thiol [54] and functionalization via addition reactions [55] have also been studied
14 to enhance efficiency of modification.

15 Azo-azomethines offer an electron rich phenolic skeleton in combination with two
16 different Brønsted basic sites, desirable features of a PA host. The azomethine group itself
17 allows for easy incorporation of the host in a system with suitable tether (e.g., a linker
18 connected with a silanizing unit) for immobilization on silica surfaces. To the best of our
19 knowledge, solid surfaces functionalized with azo-azomethine hosts still need to be explored
20 for the adsorption of PA. Hence, an azo-azomethine host is developed for the decoration of
21 silica with its Brønsted-basic sites and π -basic moieties for proton transfer with PA to
22 eventually furnish electrostatic host-guest interactions. Being attached to a silatrane
23 functionalized linker, this host allows for convenient silanization of amorphous silica.
24 Previously, we reported silatranes (tricyclic analogues of triethoxysilanes) as modifiers for
25 functionalizing silica surfaces which are superior to related triethoxysilanes [56,57]. In the
26 present report, synthesis and characterization of the azo-azomethine host (H), the study of its
27 host-guest (H-G) interaction, functionalization of sol-gel derived silica, optimized PA
28 adsorption conditions, studies on efficiency over structurally related guests, and validation
29 parameters of the herein developed method are reported in detail.

30 **2. Experimental**

31 **2.1 Materials**

32 Toluene (Fischer Scientific) and diethyl ether (Fischer Scientific) were distilled from
33 sodium/benzophenone before use and stored over molecular sieves for 24 h under nitrogen

1 atmosphere. Methanol (Finar), ethanol absolute (Merck), dichloromethane (Fischer
2 Scientific), p-nitrophenol (TCI), 2,4-dinitrophenol (Aldrich), polyethyleneglycol (Acros),
3 tetraethylorthosilicate (Acros), nitrobenzene (Sd-fine), aniline (Merck), phenol (Sd-fine),
4 picric acid (Aldrich), 2-hydroxyacetophenone (Acros), sodium carbonate (Merck), sodium
5 nitrite (Qualigens), cetyltrimethylammonium bromide (CDH), 3-
6 aminopropyl(triethoxy)silane (Aldrich), triethanolamine (Merck), concentrated hydrochloric
7 acid (National Chemical) and concentrated nitric acid (National Chemical) were used as such
8 without any purification. 3-aminopropylsilatrane was synthesized from 3-
9 aminopropyl(triethoxy)silane and triethanolamine as reported earlier [58].

10 **2.2 Physical measurements**

11 Infrared spectra were routinely obtained on Thermo scientific NICOLET IS50 FT-IR
12 and Perkin Elmer RX-I FT IR spectrophotometers. Mass spectral measurements (ESI source
13 with capillary voltage 2500 V) were carried out on a VG Analytical (70-S) spectrometer. C,
14 H, N elemental microanalyses were obtained on a FLASH-2000 organic elemental analyzer.
15 Solution NMR (^1H , ^{13}C) spectra were recorded at 25 °C on a Bruker Avance II FT NMR (AL
16 400 MHz) and on a JEOL (300 MHz) spectrometer. Chemical shifts in ppm are reported
17 relative to tetramethylsilane (TMS). Single-crystal X-ray structure analysis was carried out on
18 a Stoe IPDS-2T diffractometer using Mo $K\alpha$ -radiation ($\lambda = 0.71073 \text{ \AA}$). The structure was
19 solved by direct methods (SHELXS-97) and refined with full-matrix least-squares method
20 (refinement of F^2 against all reflections with SHELXL-97). Electronic spectral measurements
21 were carried out using a JASCO V-530 double beam spectrophotometer in the range 250-600
22 nm using quartz cells (1 cm). The Brunauer–Emmett–Teller (BET) surface area was
23 estimated using a NOVA 2000e BET surface area analyzer (Quantachrome, USA) using
24 multiple point measurement. Prior to BET analysis, degassing of the samples was done at 150
25 °C for 10 h. Thermogravimetric analysis was carried out in dynamic nitrogen atmosphere
26 using a TA Q600 analyzer at a heating rate of 20 K min^{-1} . Pore size distributions were
27 calculated by the Barrett-Joyner-Halenda (BJH) method. Morphology of the adsorbent was
28 investigated by SEM SU8010 and high resolution transmission electron microscope at 200
29 kV voltage using an FP 5022/22-Tecnai G2 20 S-TWIN instrument. A Supelco Visiprep solid
30 phase extraction chamber equipped with a vacuum pump (15 mmHg) was used for some
31 optimization experiments.

32 **2.3 Synthesis of the azo-azomethine host (H)**

33 The azo-azomethine host was synthesized in a two step procedure. In the first step, the
34 azo dye was synthesized according to a well-known method [59]. In brief, aniline (2.3 mL, 25

1 mmol) was dissolved in conc. hydrochloric acid (6.0 mL) and heated in a beaker to form a
 2 clear solution. This solution was cooled in an ice/salt bath (to 0-5 °C) and aqueous solution of
 3 sodium nitrite (2.0 g, 28 mmol dissolved in 10 mL water) was added drop-wise keeping the
 4 temperature of the reaction mixture in the same range. The contents were stirred for 30 min
 5 (at 0 °C) followed by the drop-wise addition of 2-hydroxyacetophenone (2.6 mL, 25 mmol)
 6 and the resulting mixture was stirred for 2 h (at 0-5 °C). The orange precipitate (**azo dye**)
 7 thus formed was filtered and recrystallized from ethanol. In the second step (for silyl
 8 functionalization) 3-aminopropylsilatrane (0.50 g, 2.15 mmol dissolved in 10 mL toluene)
 9 was added to a single-neck round bottom flask fitted with a Dean-Stark trap. To this solution,
 10 **azo dye** (0.517 g, 2.15 mmol) in toluene (30 mL) was added drop-wise using a syringe. The
 11 contents were refluxed and water produced during the reaction was removed azeotropically.
 12 The contents were cooled to room temperature and toluene was removed under vacuum to
 13 afford a solid product. The orange solid was washed with diethyl ether and dried. Suitable
 14 crystals for single-crystal X-ray diffraction were obtained from a solution of the product in
 15 dichloromethane/hexane mixture by slow evaporation at room temperature.

16 2.3.1 5-Phenylazo-1-(2-hydroxyphenyl)ethanone (Azo dye)

17 Yield: 3.88 g (16.2 mmol, 65%). M.p.: 120-125 °C; ¹H NMR (CDCl₃, 300 MHz): δ
 18 (ppm) 2.75 (s, 3H, COCH₃), 7.05 (d, 1H¹¹, J = 8.7 Hz), 7.45 (m, 3H^{3,4,5}), 7.85 (d, 2H^{2,6}, J =
 19 8.1 Hz), 8.08 (dd, 1H¹², J = 9 Hz), 8.32 (d, 1H⁸, J = 2.1 Hz), 12.5 (s, 1H, OH); IR (cm⁻¹):
 20 1540 ν (-N=N-), 1636 ν (C=O), 3186 ν (O-H).

21 2.3.2 4-Phenylazo-2-{1-[3-(2,8,9-trioxa-5-aza-1-silabicyclo[3.3.3]undec-1yl)propylimino]- 22 ethyl}-phenol (H)

23 Yield: 0.65 g (1.44 mmol, 72%). M.p.: 150-155 °C; ¹H NMR (400 MHz, CDCl₃): δ
 24 (ppm) 0.44 (m, 2H, SiCH₂), 1.83 (m, 2H, CCH₂C), 2.48 (s, 3H, NCCH₃), 2.71 (t, 6H,
 25 NCH₂C, J = 5.8 Hz), 3.54 (t, 2H, CCH₂N), 3.66 (t, 6H, OCH₂, J = 5.8 Hz), 6.78 (d, H¹¹, J =
 26 9.2 Hz), 7.30-7.42 (m, 3H^{3,4,5}), 7.75 (d, 2H^{2,6}, J = 7.4 Hz), 7.90 (dd, 1H¹², J = 9.24 Hz), 8.05
 27 (d, 1H⁸, J = 2.5 Hz), 17.06 (s, 1H, OH); ¹³C NMR (100.68 MHz, CDCl₃): δ (ppm) 13.77
 28 (SiCH₂), 25.28 (CCH₂C), 49.1 (NCCH₃), 51.18 (CCH₂N), 57.78 (NCH₂), 60.73 (OCH₂),
 29 114.8 (C¹¹), 119.8 (C^{2,6}), 122.2 (C⁸), 124.3 (C⁹), 125.8 (C¹²), 130.4 (C^{3,5}), 138.8 (C⁴), 141.3
 30 (C⁷), 153.0 (C¹), 173.3 (C=N), 177.0 (C¹⁰); IR (solid state, cm⁻¹): 582 m (ν Si←N) 706 s,
 31 758 s (ν_s Si-O), 847 m, 873 w (ν C-N), 907 m (ν_s NC₃), 936 m (ν C-C), 954 w, 1016 s, (ν_{as}
 32 NC₃), 1095 vs (ν_{as} Si-O), 1125 vs (ν C-O), 1171 m (τ CH₂O), 1273 m (ω CH₂O), 1353 m,
 33 1400 w (δ CH₃C), 1464 (ν C=C), 1549 (-N=N-), 1605 vs (ν C=N), 2872 s, 3035 (ν_s CH₂),
 34 3186 b (N-H---O); MS (% relative abundance, m/z fragment): 174 (3.45, N(CH₂CH₂O)₃Si)⁺,

1 455.2 (100, M + H)⁺, 477.2 (38.78, M + Na)⁺, 478.2 (9.94, M + H + Na)⁺, 931 (3.55,
2 2M+Na); Anal. Calcd for C₂₂H₃₂N₄O₄Si: C, 61.51; H, 6.88; N, 11.96; Found: C, 59.83; H,
3 6.63; N, 12.00.

4 Single-crystal X-ray diffraction analysis, selected parameters of data collection and
5 structure refinement: empirical formula C₄₇H₆₂Cl₂N₈O₈Si₂ (*FW* 994.12), *T* 180(2) K, λ
6 0.71073 Å, triclinic, *P*-1, *a* 6.7621(6), *b* 13.2927(12), *c* 14.9421(15) Å, α 65.933(7), β
7 82.804(8), γ 89.464(7) deg, *V* 1215.4(2) Å³, *Z* 1, ρ_{calc} 1.358 Mg/m³, μ_{Mokua} 0.245 mm⁻¹, *F*
8 (*000*) 526, *Reflections collected* 11328, *Unique* 4504 [R(int) 0.0406], θ_{max} 25.5 deg,
9 *Completeness* 99.7%, *Data/restraint/parameters* 4504/7/321, *GoF on F²* 1.072, *R₁ [I > 2σ(I)]*
10 0.0607, *R₁ (all data)* 0.1419, *wR₂ (all data)* 0.1382.

11 **Decoration of silica with host (H@SM)**

12 The functionalized silica decorated with host sites was prepared in two steps including
13 1) Fabrication of the mesoporous silica monolith 2) Incorporation of azo-azomethine hosts.
14 Firstly, a mesoporous silica monolith was synthesized by the sol-gel method as reported in
15 literature [60]. Briefly, tetraethylorthosilicate (5.58 g, 26.7 mmol, 6.0 mL) was added to a
16 solution of polyethyleneglycol (5.0 g, 0.142 mmol) in aqueous nitric acid (0.165 M, 30 mL)
17 and the contents were stirred. As a clear solution had formed, CTAB (1.0 g, 2.74 mmol) was
18 added and stirring was continued until the surfactant was completely dissolved to form a sol
19 solution. The obtained sol was left for gelation and subsequently aged for 48 h at 40 °C to
20 afford a gel. To procure large textural pores, the gel was kept in 1 M NH₄OH (2 mL) solution
21 for 9 h at 90 °C and then acidified with a 0.1 M HNO₃ solution (approx. 10-15 mL). The
22 obtained solid was washed several times with water and ethanol, and dried for 3 days at 60
23 °C in an open beaker. The material was subsequently calcined at 550 °C for 5 h and was
24 thereafter ground properly.

25 In the second step, calcined mesoporous silica from a finely ground monolith (0.5 g)
26 was dispersed in 20 mL ethanol followed by the addition of an ethanolic solution of host (0.5
27 g in 10 mL ethanol). To the above mixture, 0.3 mL of aqueous ammonia (25% w/v) was
28 added and the mixture was stirred at 35 °C for 24 h under inert atmosphere. The resulting
29 product was separated by centrifugation and the unreacted host was extracted with
30 dichloromethane using a Soxhlet apparatus. The obtained light yellow silica decorated with
31 azo-azomethine host sites (H@SM) was dried under vacuum for 30 min and characterized by
32 IR (as KBr pellet), SEM, HR-TEM, BET and elemental analysis.

33 **2.4 Adsorption of picric acid on H@SM**

1 The H@SM obtained along the above mentioned protocol was employed as sorbent for the
 2 adsorption of picric acid (PA). The batch method was used to optimize the adsorption
 3 conditions such as temperature and weight of adsorbent: H@SM was stirred with 5 mL of PA
 4 solution for about five min to attain equilibrium, and then filtered. Further experiments, such
 5 as adsorption isotherm and recovery and reuse studies were carried out by filling the sorbent
 6 in a solid phase extraction (SPE) cartridge. In this method, 5 mL of PA solution with varying
 7 concentrations ($0.15 \text{ mmol}\cdot\text{L}^{-1}$ to $0.65 \text{ mmol}\cdot\text{L}^{-1}$) were passed through the SPE cartridge
 8 packed with 20 mg of H@SM at a pressure of 15 mmHg. From the filtrate a UV/Vis
 9 spectrum was recorded to determine the amount of PA left in the solution. The adsorption
 10 amount (Q_e , $\text{mmol}\cdot\text{g}^{-1}$) was calculated according to equation (1) where C_o is the initial
 11 concentration of PA ($\text{mmol}\cdot\text{L}^{-1}$), C_e is the concentration of PA at adsorption equilibrium
 12 ($\text{mmol}\cdot\text{L}^{-1}$), V is the volume of PA solution (0.005 L), and M is the weight of the adsorbent
 13 H@SM (0.02 g).

$$14 \quad Q_e = V(C_e - C_o)/M \quad (1)$$

15 **2.5 Regeneration of H@SM and recovery of PA**

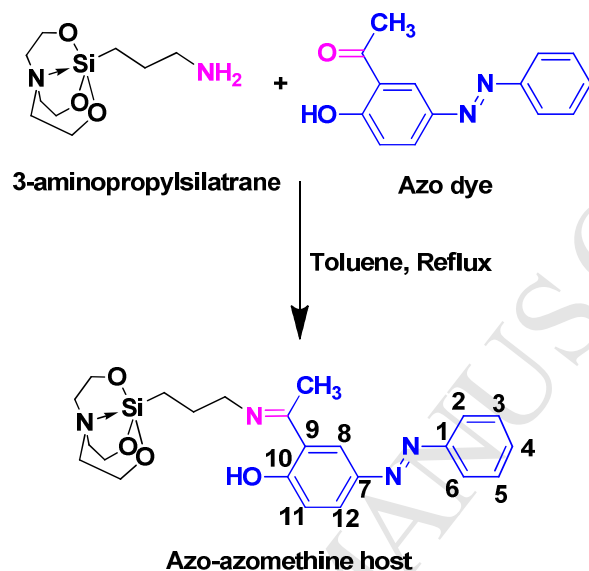
16 To evaluate the reusability of H@SM, PA (0.15 mM solution) was passed through the
 17 H@SM equipped SPE cartridge under reduced pressure (15 mmHg). The concentration of PA
 18 left in the solution after passing through the SPE cartridge was measured by UV/Vis
 19 spectroscopy at 353 nm. The cartridge was dried for 15 min and then acetonitrile (12 mL)
 20 was passed to elute the adsorbed PA. In the eluent the amount of desorbed PA was
 21 determined using UV/Vis spectrophotometry. The operation was repeated for five times using
 22 the same H@SM for adsorption-desorption of PA. The data obtained was used to calculate
 23 recovery of PA in acetonitrile and adsorption capacity of H@SM in the subsequent cycles.

24 **3 Result and Discussion**

25 Picric acid (PA) is highly acidic and thereby transfers its proton to an electron rich
 26 site of a basic scaffold to form an acid-base pair which is held together by electrostatic
 27 interaction of its ionic components and by hydrogen bonding. Based on this concept, we
 28 designed a sorbent with electron rich hosts for the uptake of PA by ion-pair formation. In this
 29 work, an azo dye was synthesized and a silanizing unit was incorporated as a side chain via
 30 azomethine linkage to obtain an azo-azomethine host (H) (**Scheme 1**).

31 The hosts were uniformly transferred into the meso-pores and attached to the surface
 32 OH groups of the silica via controlled hydrolytic cleavage of the silatrane cage in basic
 33 conditions. Thus, during silanization propyl chains with host pendants were condensed via

1 silanol groups and occupied sites in the meso pores of the three dimensional silica network.
 2 These pendants bulged outwards with donor sites in such a way that they can be exposed to
 3 the target (PA). The mesoporous nature of the silica helps in the percolation of PA through
 4 the channels for easy access of the host, thereby enhancing the adsorption efficiency of
 5 H@SM.



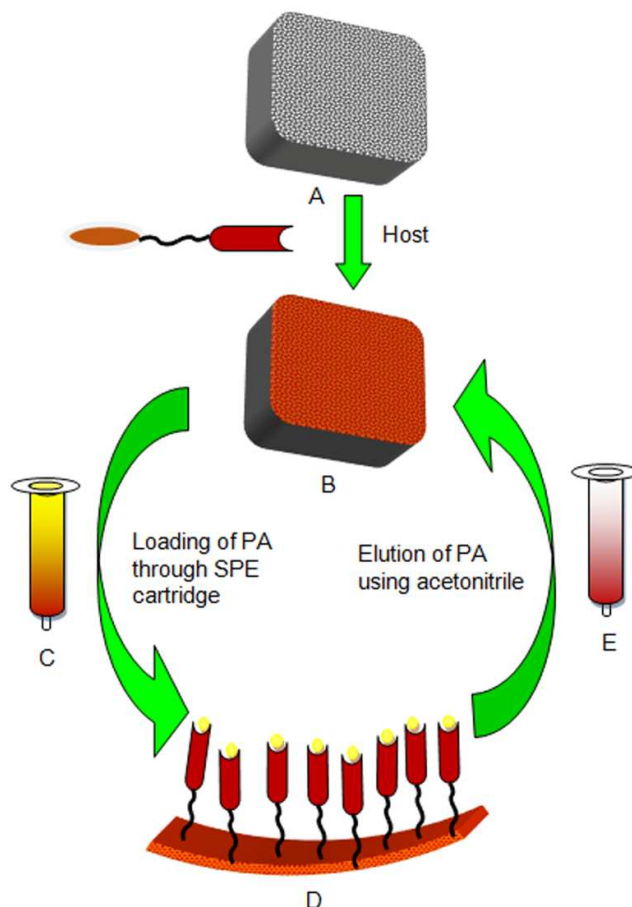
6
 7 **Scheme 1 Silanization of host via azomethine linkage.**

8 The adsorption of PA onto H@SM was studied by stirring (batch process) as well as
 9 by loading the material in a solid phase extraction (SPE) cartridge. In both modes, uptake of
 10 PA was very rapid and equilibrium was achieved very quickly. The adsorption studies using
 11 SPE were preferred over batch process to prevent the loss of adsorbent during filtration, to
 12 reduce the equilibration time, and to enhance the interaction between host and guest during
 13 percolation in channels under vacuum. The overall operation, i.e. fabrication of H@SM,
 14 loading into the SPE cartridge, adsorption and desorption of PA and regeneration of H@SM,
 15 are illustrated in **Figure 1**.

16 3.1 Proposed mechanism for host-guest interaction

17 Various studies were carried out to propose a mechanism involved in the adsorption of PA.
 18 Firstly, the host-guest interactions were studied by mixing the azo-azomethine host (H) and
 19 picric acid (PA) in different equivalents to observe the change in a UV/Vis absorption band.
 20 The equimolar mixing of host and guest at lower concentrations (below 0.12 mM) exhibited
 21 no significant change in the UV/Vis spectrum of the mixture; however, above 0.12 mM
 22 concentration it showed origin of low energy band (at around 460 nm) as a shoulder. With the
 23 further increase in the concentration, the color of the solution changed from yellow to bright

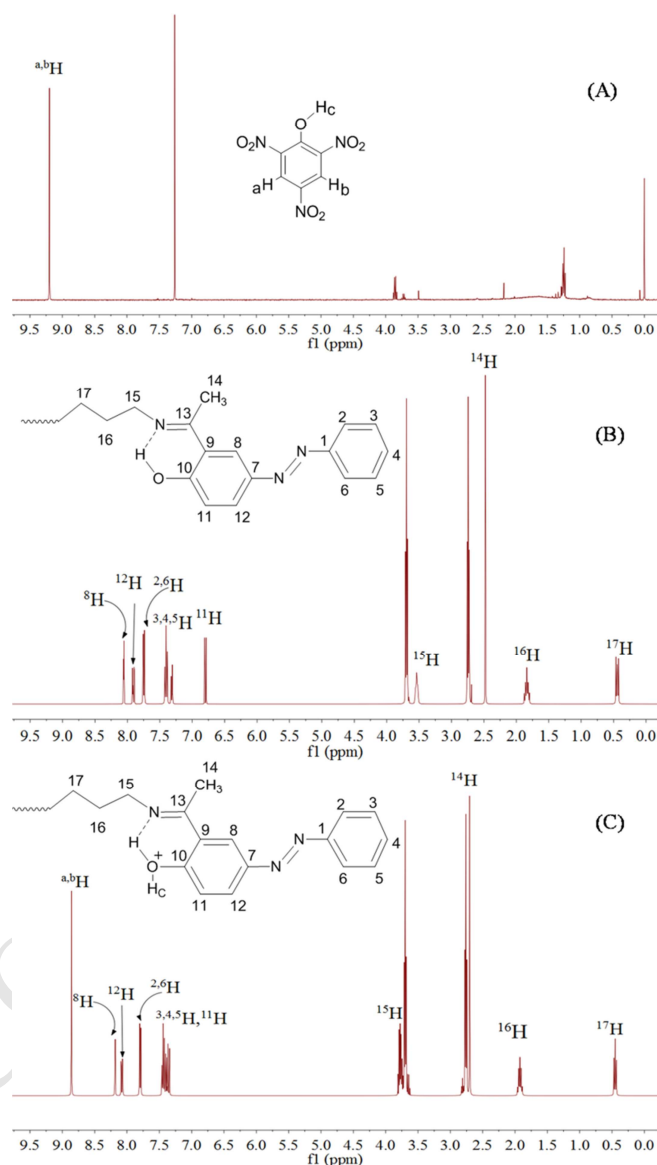
1 red with the broadening of shoulder (**Figure S1**). This indicated the formation of ion-pairs
 2 between PA (guest) and the azo-azomethine host (H).



3
 4
 5 **Figure 1** An illustration representing the complete procedure (A) SM (B) H@SM (C) SPE
 6 cartridge loaded with H@SM (D) Interaction between host (H) and guest (PA) (E) SPE
 7 cartridge with H@SM after desorption of PA.

8 Secondly, the shifting of ^1H NMR signals of equimolar solutions of host and guest
 9 revealed the transfer of the acidic proton from PA to the host molecule. An upfield shift (by
 10 0.35 ppm) in the aromatic protons (H_a and H_b) of PA corroborated the proton transfer. The
 11 disappearance of the proton signal at 17.0 ppm (azomethine O-H-N intramolecular hydrogen
 12 bond) and appearance of a signal at 13.40 ppm substantiated the shifting of the proton from
 13 PA (which is also supported by various literature reports [20-23]). To confirm the protonation
 14 as the cause of ^1H NMR spectroscopic observations, the interaction of trifluoroacetic acid
 15 (TFA) with the host was also studied by recording ^1H NMR spectra. The similar shifting of
 16 the proton signals in H-PA and H-TFA interactions revealed proton transfer in both cases. An
 17 increasing order of downfield shift observed in the aromatic protons of host in the presence of

1 PA/TFA can be written as $^{2,6}\text{H}$ (0.06/0.08) < $^{3,4,5}\text{H}$ (0.08/0.16) < ^8H (0.13/0.19) < ^{12}H
 2 (0.17/0.23) < ^{14}H (0.23/0.22) < ^{15}H (0.24/0.28) < ^{11}H (0.56/0.66). The host molecule possesses
 3 three electron rich sites, and therefore the proton can be transferred either to the azomethine
 4 group (C=N or OH) or to one of the N=N sites. As the shifting of ^1H NMR signals showed
 5 maximum differences for the signal of ^{11}H , protonation of the OH site (with formation of N-
 6 H...O-H motif) appears most likely (**Figure 2**).

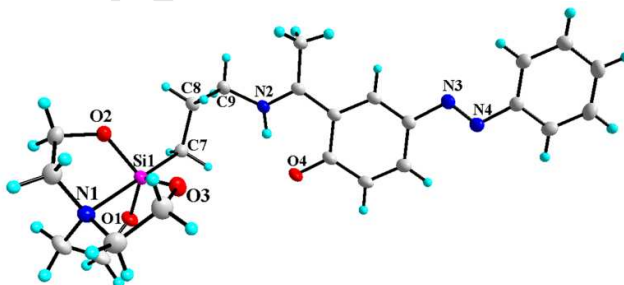


7
 8 **Figure 2** Change in chemical shift of aromatic signals of host and guest before and after
 9 mixing of equimolar concentrations (A) ^1H NMR of picric acid (B) ^1H NMR of host (C)
 10 Proposed cationic species upon proton transfer from picric acid to host.
 11 **3.2 Characterization of host, SM and H@SM**

1 The IR spectrum of the host showed a strong C=N stretching at 1605 cm^{-1} (at lower
2 value due to H-bonding), broad OH stretching positioned between $3200\text{-}3400\text{ cm}^{-1}$, and N=N
3 stretching at 1549 cm^{-1} . In the ^1H NMR spectrum, characteristic peaks of the tricyclic
4 silatranyl moiety appeared at 2.71 and 3.66 ppm due to NCH_2 and OCH_2 groups, respectively
5 (**Figure S2-S4**).

6 According to the proposed mode of interaction (proton transfer), both the $-\text{NO}_2$ and $-\text{OH}$
7 groups (and the high acidity of PA, which results therefrom) are responsible for the host-
8 guest interactions. Similar tests on structurally related species lacking either nitro and/or
9 hydroxyl group(s) such as 2,4-dinitrophenol (2,4-DNP), p-nitrophenol (4-NP), m-nitrophenol
10 (m-NP), phenol (PH), and nitrobenzene (NB) indicated significantly weaker interaction with
11 the host. In all the cases, very low (2,4-DNP, p-NP and m-NP) or no adsorption (PH and NB)
12 was attained (**Table S1**). Accordingly, fast uptake of PA can be ascribed to proton transfer
13 from guest (PA) to host molecule.

14 The mass spectrum of the azo-azomethine host exhibited the corresponding molecular
15 ion peak at 455.2 m/z . The molecular structure of the host was elucidated by single crystal X-
16 ray diffraction (selected parameters are summarized in **characterization of H**). In the crystal
17 packing, long organic chains containing aromatic rings planted with azo and azomethine
18 groups are projected away from the silanizing unit (**Figure 3**). The molecule showed
19 stabilization as keto-enamine isomer, which could be attributed to the intramolecular proton
20 transfer. Similar orientation of donor sites could be expected for the host moieties enclosed
21 within the silica. Hence, host sites are easily accessible by the guest during adsorption.

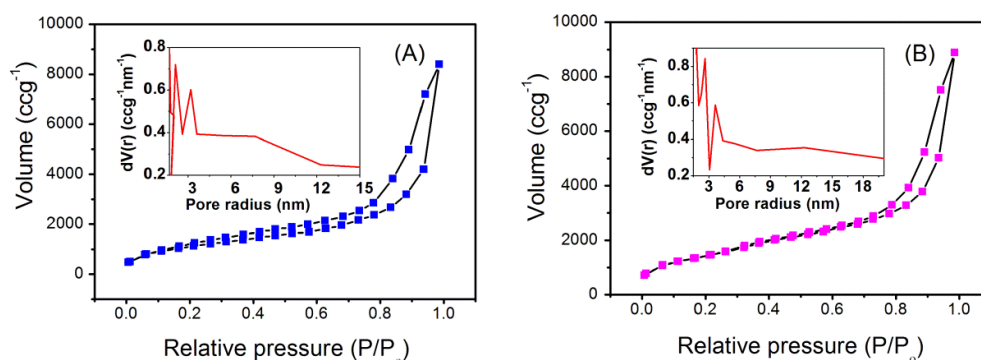


22
23 **Figure 3** Molecular structure of the host (H), [Ellipsoids are shown at the 40% (C, N, O and
24 Si-atoms) and 10% probability level (H-atoms)]. Selected bond lengths [\AA] and angles [deg]
25 are summarized in **Table S2** of the Supporting Information.

26 Ground silica monolith (SM), before and after functionalization (H@SM), was
27 characterized by IR, TGA, SEM, TEM, BET and elemental analysis. The FT-IR spectra of
28 SM and H@SM exhibited absorption peaks at 471, 804, 962 and $1065/1096$ (SM/H@SM)
29 cm^{-1} corresponding to Si-O-Si bending and stretching. However, H@SM exhibited a broad

1 band at 3461 cm^{-1} ascribed to the O-H stretching vibration, and sharp band at 1638 cm^{-1} due
 2 to C=N stretching, corroborating the functionalization of SM with azo-azomethine hosts
 3 (**Figure S5**). Moreover, elemental analyses of H@SM supported the results and showed the
 4 presence of C (5.95%) and N (1.26%), which were completely absent in SM.

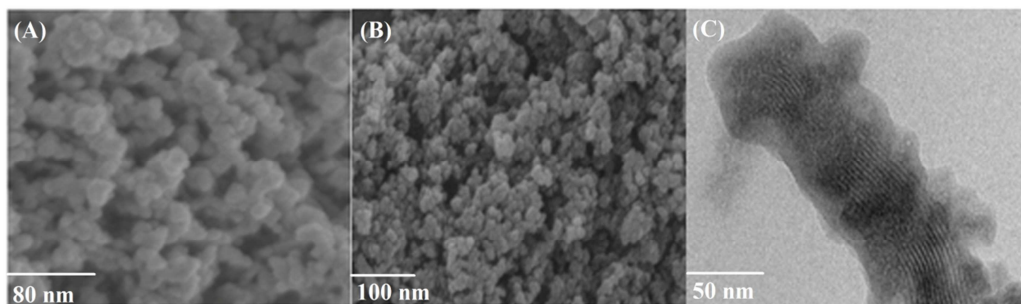
5 To determine the pore volume, pore diameter and surface area, N_2 adsorption-
 6 desorption isotherm measurements were performed for both SM and H@SM. Both curves
 7 follow the type IV adsorption behavior with H3 hysteresis loop. The upper curve follows the
 8 adsorption while the lower curve follows the desorption process. The hysteresis loop of both
 9 SM and H@SM demonstrates the mesoporous nature of materials, given in **Figure 4**. The
 10 slight decrease in surface area of H@SM ($1606\text{ m}^2\cdot\text{g}^{-1}$) compared to SM ($1814\text{ m}^2\cdot\text{g}^{-1}$)
 11 depicted the immobilization of host into the SM. Pore size distribution is shown in the inset
 12 of **Figure 4** calculated from the adsorption branch using a BJH method. The sharp peaks
 13 indicate the presence of mesopores corresponding to radii 2.6 nm and 3.6 nm, and 2.2 and 3.3
 14 nm for SM and H@SM, respectively. Thermogravimetric analysis (TGA) was performed to
 15 investigate the content of organic functional groups grafted on the surface of the silica.
 16 Weight loss below $200\text{ }^\circ\text{C}$ may be attributed to loss of water from the surface of both H@SM
 17 and SM. In case of H@SM, apart from water loss, 8.23% weight loss at about 200 to $750\text{ }^\circ\text{C}$
 18 may be assigned to the loss of organic moieties. H@SM showed total 18% weight loss,
 19 which revealed that the remaining part of the adsorbent is composed of silica only and
 20 remained unaffected even at $1000\text{ }^\circ\text{C}$. The TGA curve for the host is shown in **Figure S6** for
 21 comparison. A similar pattern was observed for the weight loss in host and H@SM.



22
 23 **Figure 4** N_2 adsorption/desorption isotherms of H@SM (A) SM (B) and pore-size
 24 distribution [inset of (A), (B)].

25 FE-SEM images of both the functionalized and non-functionalized silica surfaces
 26 revealed homogeneity of skeleton size. Surface morphology of the silica remained the same
 27 after immobilization, which indicates uniform coating of the organic functionality on the

1 silica surface. A TEM image of H@SM recorded by falling electron beam perpendicular to
 2 the pore axis represents regular parallel rows in H@SM indicating the porous nature of this
 3 adsorbent (**Figure 5**).



4 **Figure 5** SEM images of SM and H@SM (A and B); HR-TEM image of H@SM (C).

6 3.3 Optimization of adsorption parameters

7 3.3.1 Effect of amount of coated adsorbent

8 For this experiment, different amounts of H@SM were stirred with 5 mL of PA
 9 solution (0.075 mM) for 5 min. The effect of different quantities of adsorbent ranging from
 10 0.001 to 0.02 g on the adsorption equilibrium is shown in **Figure S7A**. It clearly showed
 11 increase in the adsorption of PA with the increase in the amount of H@SM from 0.001 to
 12 0.015 g. The adsorption of PA became constant (nearly 99%) for the 0.015-0.02 g of H@SM.
 13 Hence, the 0.02 g of H@SM was used for the further experiments.

14 3.3.2 Effect of temperature

15 The effect of the solution temperature on the adsorption of PA was investigated
 16 between 15 °C to 45 °C. The studies were performed by stirring 5 mL of PA solution (0.15
 17 mM) with 0.02 g adsorbent for 5 min at different temperatures (**Figure S7B**). No subsequent
 18 change in the uptake of PA was observed with the increase in temperature. Therefore, further
 19 adsorption studies were performed at 30 °C.

20 3.3.2 Adsorption isotherms

21 Langmuir and Freundlich isotherm were studied in detail to check the surface
 22 properties of the adsorbent. The isotherm constants were determined using the linear
 23 regression method (**Figure 6 bottom**).

24 *Langmuir Model*

25 The adsorption capacity and equilibrium constants for the adsorption of PA were calculated
 26 from Langmuir and Freundlich adsorption isotherms. The linear form of the Langmuir
 27 isotherm can be represented as:

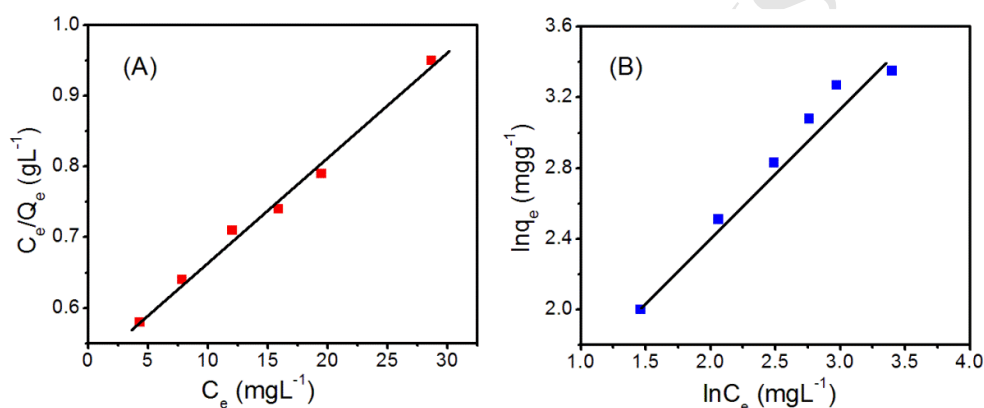
$$28 \quad C_e/Q_e = C_e/Q_m + 1/K_L/Q_m \quad (2)$$

1 where C_e ($\text{mmol}\cdot\text{L}^{-1}$) and Q_e ($\text{mmol}\cdot\text{g}^{-1}$) are concentration and adsorption amount of PA,
 2 respectively at adsorption equilibrium, Q_m ($\text{mmol}\cdot\text{g}^{-1}$) and K_L ($\text{L}\cdot\text{mmol}^{-1}$) are the theoretical
 3 maximum adsorption capacity and the Langmuir equilibrium constant related to theoretical
 4 maximum adsorption capacity and energy of adsorption, respectively. The experimental data
 5 was plotted against C_e/Q_e versus C_e according to equation (1) (**Figure 6A**).

6 The dimensionless constant separation factor or equilibrium parameter, R_L related to
 7 the Langmuir isotherm can be defined as given in eq. (3).

$$8 \quad R_L = 1/(1+K_L C_e) \quad (3)$$

9 For a favourable process the value of R_L should be less than 1 and more than 0. The
 10 calculated R_L value for adsorption of PA on adsorbent is 0.028, which indicates the
 11 favourable adsorption.



Langmuir Model			Freundlich Model			
Q_m ($\text{mg}\cdot\text{g}^{-1}$)	K_L ($\text{L}\cdot\text{mg}^{-1}$)	R^2	R_L	K_f ($\text{L}^{1/n} \text{mg}^{(1-1/n)} \cdot \text{g}^{-1}$)	n	R^2
68.5	0.03	0.99	0.028	2.56	1.37	0.98

12
 13 **Figure 6** (A) Langmuir and (B) Freundlich isotherms for the adsorption of PA on H@SM
 14 (Bottom: Adsorption isotherm parameters determined from experimental data.)

15 *Freundlich isotherm*

16 The Freundlich isotherm assumes multilayer adsorption. The linear form of the
 17 Freundlich model can be written as follows:

$$18 \quad 1/Q_e = \ln K_f + 1/n \ln C_e \quad (4)$$

19 K_f , the constant of the Freundlich isotherm ($\text{L}^{1/n} \text{mg}^{(1-1/n)} \cdot \text{g}^{-1}$) and $1/n$, the Freundlich
 20 exponent, represent adsorption capacity and adsorption intensity, respectively. The constants
 21 were calculated from intercept and slope of the plot between $\ln Q_e$ versus $\ln C_e$. Regression
 22 coefficient were found to be close to unity revealing the well fitting of adsorption data in

1 Freundlich adsorption isotherm (**Figure 6B**). The value of n is higher than 1 indicating the
2 favourable process.

3 **3.4 Recovery and reuse Studies**

4 To check the reusability of the adsorbent, PA (0.15 mM) was adsorbed on the
5 mesoporous adsorbent (0.020 g) followed by the elution process using acetonitrile (for five
6 repetitions) and adsorption efficiency was calculated for each cycle. Removal efficiency was
7 investigated by taking the ratio of the amount of PA recovered to the amount of PA adsorbed.
8 Each cycle showed 89-90% recovery of PA with 8 mL of acetonitrile (eluting solvent). No
9 change was observed in the adsorption capacity of the adsorbent for at least three cycles
10 (**Figure S8**), which indicates that the adsorbent can be reused.

11 **3.5 Adsorption of other nitro phenols**

12 Uptake of PA was compared with its structural analogues, adsorption studies of related
13 compounds such as nitrophenols (2,4-DNP, o-NP, p-NP), nitrobenzenes (p-NT, NB) and
14 phenol (PH) were carried out. NB, p-NT and PH did not show any adsorption ($Q_e = 0$), while
15 ortho and para nitrophenols showed little adsorption relative to 2,4-DNP (**Figure S9**). It
16 revealed that adsorption of PA is more efficient relative to other phenols.

17 **3.6 Comparison with reported methods**

18 The presented method is compared with existing methods for PA adsorption in terms of
19 maximum adsorption capacity, time required for attaining adsorption equilibrium and
20 temperature (data are summarized in **Table S3**) [21-24,26,61-63]. The results revealed that
21 silica surface decorated with azo-azomethine host fabricated in the present method exhibits
22 better adsorption capacity (Q_m) than the existing adsorbents except activated carbon,
23 hydrotalcite (HT)/calcined hydrotalcite (HT-500) and uncalcined mesoporous silica.
24 However over other nitro-aromatics, the presented method is also better over existing
25 methods in terms of selectivity and the short time required to achieve adsorption equilibrium,
26 thus facilitating the fast uptake of PA. This sorbent is suitable for solid phase extraction of
27 PA using batch method as well as cartridge. Its use in conjunction with solid phase cartridge
28 prevents the loss of adsorbent during filtration and makes the method rapid.

29 **3.7 Conclusion**

30 The study illustrates the designing and engineering of sol-gel derived (initially
31 monolithic) silica with azo-azomethine pendants for the fast uptake of picric acid (PA) via
32 formation of intermolecular hydrogen bonding followed by proton transfer. The temperature
33 of the test solution has no effect on the adsorption of PA and adsorption/desorption process
34 occurs very fast at room temperature when H@SM is loaded in SPE cartridge. The adsorption

1 isotherm follows both Freundlich and Langmuir model with maximum adsorption capacity of
2 68.5 mg·g⁻¹. The adsorbed PA can be recovered from the H@SM using acetonitrile as eluent
3 and the sorbent can be reused for the next adsorption cycle.

4 **4. Supplementary data**

5 CCDC 1441990 contains the supplementary crystallographic data for host molecule.
6 The data can be obtained free of charge from The Cambridge Crystallographic Data Centre.

7 **5. Acknowledgement**

8 Authors are thankful to DST, New Delhi [Regd. No. CS-099/2012], DST-
9 Purse, New Delhi and CSIR, New Delhi for providing financial support.

10 **6. References**

- 11 [1] Bingham E, Cohn B, Powell CH. *Patty's Toxicology*, John Wiley & Sons: New York,
12 IIB, 980, 2000.
- 13 [2] Koopmans B, Janner AM, Jonkman HT, Sawatzky GA, Van der Woude F. *Phys Rev Lett*
14 1993;71:3569-72.
- 15 [3] Goldman ER, Anderson GP, Lebedev N, Lingerfelt BM, Winter PT, Patterson Jr CH,
16 Mauro JM. Analysis of aqueous 2,4,6-trinitrotoluene (TNT) using a fluorescent displacement
17 immunoassay. *Anal Bioanal Chem* 2003; 375:471-75.
- 18 [4] Fedoroff BT, Sheffield OE, *Encyclopedia of Explosives and Related Items*, US.
19 Department of Commerce Springfield, Virginia, 1962.
- 20 [5] J Akhavan, *The Chemistry of Explosives*, 2nd ed., Royal Society of Chemistry, London,
21 2004.
- 22 [6] Agrawal JP, *High Energy Materials, Propellants Explosives and Pyrotechnics*, Wiley-
23 VCH, Germany, 2010, p. 209-330.
- 24 [7] Favaro G, Leo DD, Pastore P, Magno F, Ballardini A. Quantitative determination of
25 chlorophenols in leather by pressurized liquid extraction and liquid chromatography with
26 diode-array detection. *J Chromatogr A* 2008;1177:36-42.
- 27 [8] Liao CJ, Chen CP, Wang MK, Chiang PN, C W Pai. Sorption of chlorophenoxy propionic
28 acids by organoclay complexes. *Environ Toxicol* 2006;21:71-79.
- 29 [9] Suliman FE, Al-Kindi SS, Al-Kindy SMZ, Al-Lawati HA. Analysis of phenols in water
30 by high-performance liquid chromatography using coumarin-6-sulfonyl chloride as a
31 fluorogenic precolumn label. *J Chromatogr A* 2006;1101:179-84.
- 32 [10] Demchenko AP, Tang KC, Chou PT. Excited-state proton coupled charge transfer
33 modulated by molecular structure and media polarization. *Chem Soc Rev* 2013;42:1379-408.

- 1 [11] Bhowmick S, Chakraborty S, Das A, Nallapeta S, Das N, Pyrazine Motif Containing
2 Hexagonal Macrocycles: Synthesis, Characterization, and Host-Guest Chemistry with Nitro
3 Aromatics. *Inorg Chem* 2015;54:8994-9001.
- 4 [12] Vishnoi P, Walawalkar MG, Sen S, Datta A, Patwari GN, Murugavel R. Selective
5 fluorescence sensing of polynitroaromatic explosives using triaminophenylbenzene scaffolds.
6 *Phys Chem Chem Phys* 2014;16:10651-8.
- 7 [13] Liu T, Zhao K, Liu K, Ding L, Yin S, Fang Y. Synthesis, optical properties and
8 explosive sensing performances of a series of novel π -conjugated aromatic end-capped
9 oligothiophenes. *J Hazard Mater* 2013;246-247:52-60.
- 10 [14] Shanmugaraju S, Mukherjee PS, π -Electron rich small molecule sensors for the
11 recognition of nitroaromatics. *Chem Commun* 2015;51:16014-32.
- 12 [15] Chowdhury A, Mukherjee PS. Electron-Rich Triphenylamine-Based Sensors for Picric
13 Acid Detection. *J Org Chem* 2015;80:4064-75.
- 14 [16] Chaudhary A, Rath SP. Encapsulation of TCNQ and the acridinium ion within a
15 bisporphyrin cavity: synthesis, structure, and photophysical and HOMO-LUMO-gap-
16 mediated electron-transfer properties. *Chem Eur J* 2012;18:7404-17.
- 17 [17] Tanaka M, Ohkubo K, Gros CP, Guillard R, Fukuzumi S. Persistent electron-transfer
18 state of a δ -complex of acridinium ion inserted between porphyrin rings of cofacial
19 bisporphyrins. *J Am Chem Soc* 2006;128:14625-33.
- 20 [18] Iqbal SA, Dhamija A, Rath SP. Metal-coordination-driven mixed ligand binding in
21 supramolecular bisporphyrin tweezers. *Chem Comm* 2015;51:14107-10.
- 22 [19] Sun X, Wang Y and Lei Y, Fluorescence based explosive detection: from mechanisms to
23 sensory materials. *Chem Soc Rev* 2015;44:8019-61.
- 24 [20] Alfonso M, Espinosa A, Tarraga A, Molina P. Multifunctional benzothiadiazole-based
25 small molecules displaying solvatochromism and sensing Properties toward nitroarenes.
26 anions, and cations, *Chemistry Open* 2014, 3, 242-49.
- 27 [21] Xu Y, Li B, Li W, Zhao J, Sun S Pang Y. ICT-not-quenching'' near infrared ratiometric
28 fluorescent detection of picric acid in aqueous media. *Chem. Commun.* 2013;49:4764-66
- 29 [22] Mondal P, Rath SP. Highly Selective and Sensitive Detection of Picric Acid explosive
30 by a bisporphyrin cleft: synergistic effects of encapsulation, efficient electron transfer, and
31 hydrogen bonding. *Eur J Inorg Chem* 2015:4956-64.
- 32 [23] Dey N, Samanta SK Bhattacharya S. Selective and Efficient Detection of Nitro-
33 Aromatic Explosives in Multiple Media including Water, Micelles, Organogel, and Solid
34 Support. *ACS Appl Mater Interfaces* 2013;5:8394-400.

- 1 [24] Kumar M, Reja SI, Bhalla V. A charge transfer amplified fluorescent Hg^{2+} complex for
2 detection of picric acid and construction of logic functions. *Org Lett* 2012;14:6084-87.
- 3 [25] Vishnoi P, Sen S, Patwari GN, Murugavel R. Charge transfer aided selective sensing and
4 capture of picric acid by triphenylbenzenes. *New J Chem* 2015;39:886-92.
- 5 [26] Sepehrian H, Fasihi J, Mahani MK. Adsorption Behavior Studies of Picric Acid on
6 Mesoporous MCM-41. *Ind Eng Chem Res* 2009;48:6772-75.
- 7 [27] Parham H, Zargar B, Rezazadeh M. Removal, preconcentration and spectrophotometric
8 determination of picric acid in water samples using modified magnetic iron oxide
9 nanoparticles as an efficient adsorbent. *Mater Sci and Eng C* 2012; 32:2109-14.
- 10 [28] Mohana D, Sarswata A, Singha VK, Francob MA, Jr. Pittman CU. Development of
11 magnetic activated carbon from almond shells for trinitrophenol removal from water. *Chem*
12 *Eng J* 2011;172:1111-25.
- 13 [29] Ganigar R, Rytwo G, Gonen Y, Radian A, Mishael YG. Polymer-clay nanocomposites
14 for the removal of trichlorophenol and trinitrophenol from water. *Appl Clay Sci* 2010;
15 49:311-16.
- 16 [30] Parham H, Saeed S. Ultrasound-assisted solid phase extraction of nitro- and chloro-
17 (phenols) using magnetic iron oxide nanoparticles and Aliquat 336 ionic liquid. *J Chromatogr*
18 *A*, 2014;1336:34-42.
- 19 [31] Uslu H, Demir G. Adsorption of Picric Acid from Aqueous Solution by the Weakly
20 Basic Adsorbent Amberlite IRA-67. *J Chem Eng Data* 2010;55:3290-296.
- 21 [32] Unuabonah EI, Taubert A. Clay-polymer nanocomposites (CPNs): Adsorbents of the
22 future for water treatment. *Appl Clay Sci* 2014;99:83-92.
- 23 [33] Jal PK, Patel S, Mishra BK. Chemical modification of silica surface by immobilization
24 of functional groups for extractive concentration of metal ions. *Talanta* 2004;62:1005-28.
- 25 [34] Y Chen, J Shi, Chemistry of Mesoporous Organosilica in Nanotechnology: Molecularly
26 Organic-Inorganic Hybridization into Frameworks. *Adv Mater* 2016;28:3235-72.
- 27 [35] Ma Q, Li Y, Su X. Silica-nanobead-based sensors for analytical and bioanalytical
28 applications. *Trend Anal Chem* 2015;74:130-45.
- 29 [36] Slowing II, Escoto JLV, Trewyn BG, Lin VSY. Mesoporous silica nanoparticles:
30 structural design and applications. *J Mater Chem* 2010;20:7924-37.
- 31 [37] Hoffmann F, Cornelius M, Morell J, Froba M. Silica-based mesoporous organic-
32 inorganic hybrid materials. *Angew Chem Int Ed* 2006;45:3216-51.
- 33 [38] Walcarius A, Mercier L. Mesoporous organosilica adsorbents: nanoengineered materials
34 for removal of organic and inorganic pollutants. *J Mater Chem* 2010;20:4478-11.

- 1 [39] Gibson LT. Mesosilica materials and organic pollutant adsorption: part B removal from
2 aqueous solution. *Chem Soc Rev* 2014;43:5173-82.
- 3 [40] Sierra I, Quintanilla DP. Heavy metal complexation on hybrid mesoporous silicas: an
4 approach to analytical applications. *Chem Soc Rev* 2013;42:3792-07.
- 5 [41] Hoffmann F, Froba M. Vitalising porous inorganic silica networks with organic
6 functions-PMOs and related hybrid materials. *Chem Soc Rev* 2011;40:608-20.
- 7 [42] Park JW, Park YJ, Jun CH. Post-grafting of silica surfaces with pre-functionalized
8 organosilanes: new synthetic equivalents of conventional trialkoxysilanes. *Chem Commun*
9 2011;47:4860-71.
- 10 [43] Tanaka N, Kobayashi H, Nakanishi K, Minakuchi H, Ishizuka N. Hierarchically Porous
11 Aminosilica Monolith as a CO₂ Adsorbent. *Anal Chem* 2001;73:420A.
- 12 [44] Ko YG, Lee HJ, Kim JY, Choi US, *ACS Appl Mater Interfaces*, 2014;6:12988-96.
- 13 [45] Ma J, Liang Z, Qiao X, Deng Q, Tao D, Zhang L, Zhang Y. Organic-Inorganic Hybrid
14 Silica Monolith Based Immobilized Trypsin Reactor with High Enzymatic Activity. *Anal*
15 *Chem* 2008;80:2949-56.
- 16 [46] Taguchi A, Schuth F. Ordered mesoporous materials in catalysis. *Microporous and*
17 *Mesoporous Mater* 2005;77:1-45.
- 18 [47] Brandhuber D, Huesing N, Raab CK, Tormaa V, Peterlik H. Cellular mesoscopically
19 organized silica monoliths with tailored surface chemistry by one-step
20 drying/extraction/surface modification processes. *J Mater Chem* 2005;15:1801-06.
- 21 [48] Triantafillidis C, Elsaesser MS, Huesing N. Chemical phase separation strategies
22 towards silica monoliths with hierarchical porosity. *Chem Soc Rev* 2013;42:3833-46.
- 23 [49] Dessources AH, Hartmann S, Baba M, Huesing N, Nedelec JM, *J Mater Chem*
24 2012;22:13-20.
- 25 [50] Huesing N, Raab C, Torma V, Roig A, Peterlik H. Periodically Mesostructured silica
26 monoliths from diol-modified silanes. *Chem. Mater* 2003;15:2690-92.
- 27 [51] Mehdi A, Reye C, Corriu R. From molecular chemistry to hybrid nanomaterials. Design
28 and functionalization. *Chem Soc Rev* 2011;40:563-74.
- 29 [52] Mouawia R, Mehdi A, Reye C, Corriu RJP. Bifunctional ordered mesoporous materials:
30 direct synthesis and study of the distribution of two distinct functional groups in the pore
31 channels. *J Mater Chem* 2008;18:4193-203.
- 32 [53] Boullanger A, Alauzun J, Mehdi A, Reye C, Corriu RJP. Generic way for functionalised
33 well-ordered cubic mesoporous silica *via* direct synthesis approach. *New J Chem.*
34 2010;34:738-43.

- 1 [54] Gobel R, Hesemann P, Friedrich A, Rothe R, Schlaad H, Taubert A. Modular Thiol–Ene
2 Chemistry Approach towards Mesoporous Silica Monoliths with Organically Modified Pore
3 Walls . Chem Eur J 2014;20:17579-89.
- 4 [55] Gobel R, Stoltenberg M, Krehl S, Biolley C, Rothe R, Schmidt B, Hesemann P, Taubert
5 A. A modular approach towards mesoporous silica monoliths with organically modified pore
6 Walls: nucleophilic addition, olefin metathesis, and cycloaddition. Eur J Inorg Chem
7 2016;2088-99.
- 8 [56] Mutneja R, Singh R, Kaur V, Wagler J, Kroke E. Development of new precursors for
9 immobilizing dyes onto silica surfaces. Dyes Pigm 2014;108:41-9.
- 10 [57] Mutneja R, Singh R, Kaur V, Wagler J, Fels S, Kroke E. Schiff base tailed silatranes for
11 the fabrication of functionalized silica based magnetic nano-cores possessing active sites for
12 the adsorption of copper ions. New J Chem 2016;40: 1640-48.
- 13 [58] Singh R, Puri JK, Sharma RP, Chahal VK, Venugopalan P. Synthesis and reactivity of
14 novel 3-isothiocyanatopropylsilatrane derived from aminopropylsilatrane: X-ray crystal
15 structure and theoretical studies. J Organomet Chem 2010;695:183-8.
- 16 [59] Albayrak C, Gumrukcuoglu IE, Odabasoglu M, Iskeleli NO, Agar E. Synthesis,
17 spectroscopic, and molecular structure characterizations of some azo derivatives of 2-
18 hydroxyacetophenone. J Mol Struct 2009;932:43-54.
- 19 [60] Smatt JH, Schunk S, Linden M. Versatile Double-Templating Synthesis Route to Silica
20 Monoliths Exhibiting a Multimodal Hierarchical Porosity. Chem Mater 2003;15:2354-61.
- 21 [61] Srivastava SK, Gupta VK, Johri N, Mohan D. Removal of 2,4,6 trinitrophenol using
22 bagasse flyash-A sugar industry waste material. Indian J.Chem Tec1995;2:33-36.
- 23 [62] Hermosin MC, Pavlovic I, Ulibarr MA, Cornejo J. Hydrotalcite as sorbent for
24 trinitrophenol: sorption capacity and mechanism. War. Res. 1996;30:171-7.
- 25 [63] Tewari BB, Mohan D, Kamaluddin. Interaction of 2,4-dinitrophenol and 2,4,6-
26 trinitrophenol with copper, zinc, molybdenum and chromium ferrocyanides. Colloids and
27 Surfaces A: Physicochemical and Engineering Aspects 1998;131:89-93.
- 28

Highlights

- Fabrication of sol-gel derived silica with azo-azomethine functionality (Host) using silatranyl moiety.
- Uptake of Picric acid (guest) via electrostatic interactions between host and guest.
- The maximum adsorption capacity of the sorbent for PA was found to be 68.5 mg.g^{-1} .